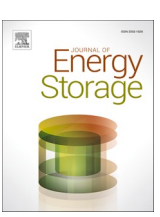
ELSEVIER

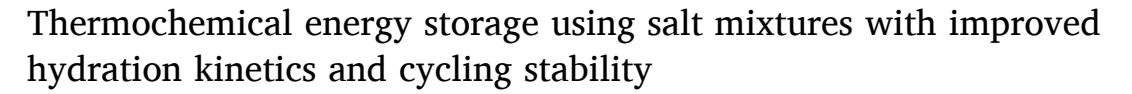
Contents lists available at ScienceDirect

Journal of Energy Storage

journal homepage: www.elsevier.com/locate/est



Research papers



Erik Barbosa, Akanksha K. Menon

George W. Woodruff School of Mechanical Engineering, Georgia Institute of Technology, Atlanta, GA 30332, USA



ARTICLE INFO

Keywords: Thermochemical materials Thermal energy storage Hydration kinetics Cycling performance Heat decarbonization Salt mixtures

ABSTRACT

Inorganic salt hydrates are promising materials for thermochemical energy storage as they undergo reversible solid-gas chemical reactions with water vapor to yield high energy densities with negligible self-discharge. However, material-level challenges such as structural and hygrothermal instabilities during the dehydration (charging) and hydration (discharging) reaction have limited their practical application in the buildings sector. The objective of this study is to address these irreversibilities in $SrCl_2$ and $MgCl_2$ by establishing a fabrication procedure that minimizes vapor diffusion resistance and lowers kinetic barriers for nucleation via particle size reduction. Furthermore, the distinct phase behavior of these two salts is leveraged to demonstrate a new binary salt mixture. Characterization of these materials was done using simultaneous thermogravimetric analysis (TGA) and differential scanning calorimetry (DSC) with a humidity generator. The results demonstrate that ball milling to particle sizes <50 μ m yields a structurally stable material with improved hydration kinetics, while a 50/50 mass ratio of the binary mixture extends the range of conditions for the hydration reaction. Importantly, the salt mixture achieves a high specific energy density of 1100 J g $^{-1}$ and peak thermal power output of 1.4 W g $^{-1}$ under conditions at which the individual salts either deliquesce (MgCl $_2$) or do not fully/rapidly hydrate (SrCl $_2$). This work provides a procedure for the standardized fabrication and rational design of thermochemical salt mixtures with complementary phase behavior.

1. Introduction

The transition from fossil fuels to a renewable energy based electric grid has been the central focus of global decarbonization efforts. However, the high penetration of renewables requires low-cost and largescale energy storage to synchronize resource availability with energy demand [1-3]. Furthermore, fossil fuels are still widely used for heating, especially in the buildings and industrial sectors [4]. For example, in the United States residential buildings sector, 60 % of the energy consumption is attributed to thermal loads such as space heating and hot water [5]. This motivates the use of thermal energy storage (TES) to decarbonize buildings by integrating renewable sources (e.g., solar heat and off-peak electricity) to deliver thermal loads on demand [6,7]. There are three types of TES technologies based on sensible heat, latent heat (phase change), and reversible thermochemical reactions. Among these, thermochemical materials (TCMs) have attracted significant attention as they can store 8-20 times more thermal energy per unit volume of material than their counterparts; this compactness is important for space-constrained applications such as buildings [8-11]. TCMs based on inorganic salt hydrates are especially of interest as they undergo a solid-gas chemical reaction with water vapor at temperatures below 100 $^{\circ}$ C (at atmospheric pressure), while being low cost and exhibiting minimal health and safety risks [6,11–13].

The process of storing and delivering thermal energy using thermochemical salt hydrates consists of two steps – charging and discharging. In the charging (dehydration) step, heat is used to drive an endothermic reaction that yields a dehydrated salt (solid) and water vapor (gas). As energy is stored within the chemical structure (heat of reaction), TCMs exhibit negligible self-discharge during storage, making them promising for seasonal or long-term energy storage [14,15]. The stored energy can then be delivered in the form of heat during the discharging (hydration) step, through an exothermic reaction between the dehydrated salt and water vapor (or moist air) that yields the hydrated salt. This reaction is expressed in Eq. 1, where MX is the solid salt, n and m represent the number of moles of water exchanged in the chemical reaction, and $\Delta_r H$ is the enthalpy (heat) of reaction.

$$MX \cdot (n+m)H_2O + \Delta_r H \leftrightarrow MX \cdot nH_2O + mH_2O$$
 (1)

As promising as salt hydrates are, the implementation of a TCM-

E-mail address: akanksha.menon@me.gatech.edu (A.K. Menon).

^{*} Corresponding author.

Nomenclature		Abbrevi	Abbreviations		
		DRH	deliquescence relative humidity (%)		
Symbol	ls	DSC	differential scanning calorimetry		
$\Delta_r H$	reaction enthalpy (J/mol)	ESD	energy storage density (J g ⁻¹)		
$\Delta_r S$	reaction entropy (J/mol-K)	PD	power density (W kg ⁻¹)		
m	mass (mg)	RH	relative humidity (%)		
MX	salt based on metal halides (-)	SEM	scanning electron microscope		
p	water vapor pressure (mbar)	STA	simultaneous thermal analysis		
p°	atmospheric pressure (mbar)	TCM	thermochemical material		
t	time (min)	TES	thermal energy storage		
T	temperature (K)	TGA	thermogravimetric analysis		
		XRD	X-ray diffraction		
Subscri	pts		•		
арр	applied	Greek s	Greek symbols		
del	deliquescence	α	hydration extent (%)		
f	final	$oldsymbol{eta}$	reaction driving force (–)		
hyd	hydration	ho	crystal density (kg/m³)		
i	initial				
r	reaction				

based storage system in a building is in its infancy owing to multiple limitations at the material level [10]. One such challenge is that the measured storage capacity - characterized using simultaneous thermal analysis (STA) – is often lower than the theoretical reaction enthalpy. This is because the experimental conditions used (i.e., heating rate, gas flow rate, and sample mass) do not account for that fact that thermodynamically favorable reactions may not commence due to kinetic limitations associated with nucleation barriers (reaction hysteresis or metastable zones) [16,17]. This results in incomplete and/or slow reactions that manifest as low energy and/or power density values, especially during hydration. Furthermore, particle size and porosity of the salt (i.e., microstructure) have also been shown to impact structural stability and reaction kinetics [18,19]. The use of different experimental parameters and the lack of standard sample fabrication renders a comparison of different salts with the literature challenging as we previously showed [20], thus limiting the rapid development of TCMs.

To extend the implementation of TCMs beyond seasonal energy storage applications, their hygrothermal stability under charge/discharge cycling must also be addressed [17,21–23]. For example, agglomeration of salt particles can occur during hydration (due to deliquescence) or dehydration (due to melting). This porosity change hinders vapor diffusion and results in slower or incomplete reactions that are not reversible, manifesting as cycling-induced performance degradation. This can be minimized to some extent by carefully selecting the reaction conditions, namely the vapor pressure (p) or relative humidity (RH) and temperature (T). However, this is challenging for salts like MgCl₂ and CaCl₂ that have a low deliquescence RH ($DRH \sim 30$ % at 25 °C) and form a salt solution in open systems where humid air is drawn from the ambient [24–26]. Similarly, salts like MgSO₄ and SrCl₂ require much higher RH (\sim 60 % at 25 °C) than what is available in most climates making it challenging to fully hydrate them [27,28].

Various approaches to make TCMs more viable have been reported in the literature, such as using a porous host matrix and adding thermally conductive fillers [25,29–34]. However, this introduces an inactive material (does not participate in the storage process), which can reduce the energy density and slow down kinetics [35,36]. Another more recent approach to improve cyclability is the use of salt mixtures; however, the handful of studies on binary mixtures reported in the literature (summarized in Table S1) do not provide a rationale for combining the two salts or insight into the mechanism that leads to improved performance [37–42]. For example, Rammelberg et al. showed that mixing MgCl₂ with CaCl₂ improved cyclability compared to the individual salts over 20 cycles [42], while Li et al. demonstrated that mixing MgSO₄ with

SrCl $_2$ improved the cyclability within 20 cycles [41]. However, the particle size of the mixed salt in the latter case was significantly smaller (~50 µm) than the individual salts (1000 µm), making a direct comparison difficult. We also note that in both these cases, salts with similar phase diagrams were mixed – MgCl $_2$ and CaCl $_2$ hydrate around 25 % RH, while MgSO $_4$ and SrCl $_2$ hydrate over 60 % RH at 25 °C [24,27,28,43] – limiting their use to a narrow range of operating conditions. More recently, Mazur et al. showed that mixing K $_2$ CO $_3$ with a deliquescent (highly hygroscopic) salt like Cs $_2$ CO $_3$ in a 20:1 mol ratio improved reaction kinetics and metastability, but no performance data (energy and power density or cycling stability) was provided and Cs $_2$ CO $_3$ is a highly toxic and corrosive salt [40].

To address these gaps, herein we report a new binary mixture of salts with different hygrothermal behavior, namely MgCl₂ (hydrates at 15–30 % RH at 25 °C) and SrCl₂ (hydrates at 50–70 % RH at 25 °C), which leverages the deliquescence of one salt to enhance the hydration kinetics of the other salt. To provide an direct comparison between the mixture and its constituent salts in terms of their thermal storage performance and stability, an experimental procedure is developed that uses (i) ball milling to a uniform particle size <50 μm , and (ii) optimized STA parameters for complete reactions to occur [18,20]. This approach is used to characterize the energy and power density of the individual salts and their binary mixture at different p-T values to establish operating conditions, followed by a hydration/dehydration cycling study to evaluate stability.

2. Materials and methods

2.1. Salt selection

SrCl₂ and MgCl₂ were chosen for this study as they have charging temperatures <80 °C and discharging temperatures ~35–50 °C that are suitable for space and water heating applications in buildings [44]. Both salts have also been characterized extensively in the literature, and their distinct phase behavior can be leveraged to form a binary mixture – MgCl₂·6H₂O has a high energy storage capacity (solid-gas reaction enthalpy), superior kinetics and low cost, but it lacks hygrothermal stability due to its low DRH (~30 % at 25 °C) [24]. Meanwhile, SrCl₂·6H₂O has a high energy density and a high hygrothermal stability (DRH ~ 70 % at 25 °C), but it requires much higher vapor pressures to hydrate that results in incomplete reactions and slower kinetics while its high cost limits application at scale [28]. These two salts were also selected because they have a common ion, which reduces the likelihood

of side reactions and byproducts (e.g., due to ion exchange or chemical interactions between the salts to form new compounds) [40].

Both salts in their hexahydrate form (99 % purity, Sigma Aldrich) were characterized at T and RH (p) values based on their respective phase diagrams shown in Fig. 1. These phase diagrams represent the Clausius-Clapeyron relation shown in Eq. (2) that establishes the equilibrium conditions for dehydration and hydration reactions of each salt [45]:

$$(n-m)ln\left(\frac{p}{p^{o}}\right) = \frac{\Delta_{r}S}{R} - \left(\frac{\Delta_{r}H}{R}\right)\frac{1}{T}$$
 (2)

where p is the vapor pressure, T is the temperature of the reaction, p° is atmospheric pressure, and $\Delta_r H$ and $\Delta_r S$ are the theoretical (equilibrium) reaction enthalpy and entropy values reported in literature [45]. Fig. 1 also shows the deliquescence curve and metastable zone associated with the hexahydrate based on literature values [16,28].

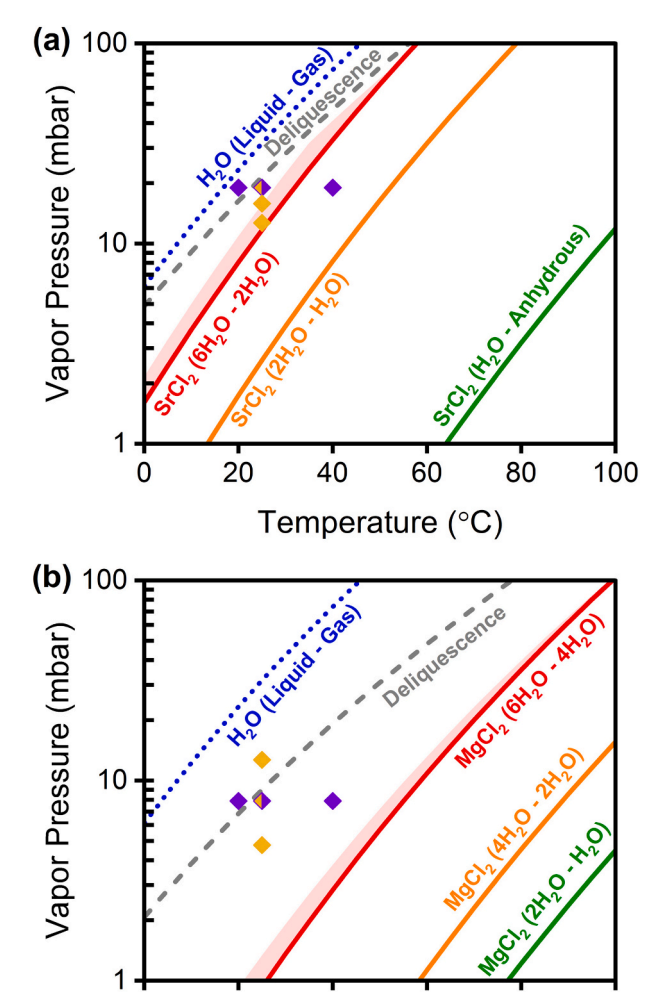


Fig. 1. Phase diagrams of (a) SrCl₂ and (b) MgCl₂ showing their different thermodynamically stable hydrates (solid curves) plotted using Eq. (2). The deliquescence of the highest hydrate (dashed curve), metastable zone of the highest hydrate (shaded region), and the liquid-vapor equilibrium for water (dotted curve) are also shown. The symbols represent experimental conditions used to evaluate the effect of temperature when vapor pressure is constant (purple diamonds), and vapor pressure when the temperature is constant (gold diamonds). (For interpretation of the references to colour in this figure legend, the reader is referred to the web version of this article.)

40

Temperature (°C)

60

80

100

0

20

2.2. Sample fabrication

The pristine salts (as received) vary in size between 500 and 1000 μm for SrCl₂·6H₂O, and 200-600 μm for MgCl₂·6H₂O (Fig. S1). To enable a direct comparison between salts, a standardized fabrication process is used. Specifically, each salt (200 mg) is first dehydrated in a vacuum oven at 105 °C overnight and then pulverized in a ball mill with five zirconia beads (3 mm diameter) for 30 min. The pulverized salts are dehydrated again in a vacuum oven at 105 °C for 1 h and then sieved to particle sizes under 50 µm. Next, the microscopic salts are preconditioned by cycling them in a vacuum oven between 105 °C (dehydration for 1 h) and an environmental chamber at 25 $^{\circ}\text{C}$ (hydration for 1 h) at an RH based on their respective phase diagrams to achieve the hexahydrate without deliquescence (25 % RH for MgCl2 and 60 % RH for SrCl2 from Fig. 1). This cycling is repeated four more times (5 cycles in total), ending in the dehydrated state for subsequent experiments. Ball milling minimizes diffusion barriers associated with larger particles (a larger surface area facilitates vapor transport and reaction kinetics [18]), while preconditioning by cycling five times equilibrates the salts for subsequent STA characterization (the first cycle is often different and not representative of material behavior). We note that MgCl₂ is in its monohydrate state and SrCl₂ is in its anhydrous state (fully dehydrated) at 105 °C; this dehydration temperature is chosen to prevent the hydrolysis of MgCl2 into HCl that occurs at 120 °C [46].

To fabricate binary salt mixtures, a homogenous solution of each salt in deionized water was first made (100 mg of pristine salt in 10 mL of deionized water). The two salt solutions are then mixed and ultrasonicated for 30 min, as shown in Fig. 2. The remaining fabrication process follows that of the individual salts, with the mixture being dehydrated in a vacuum oven at 105 °C overnight and then ball milled for 30 min. The pulverized salt mixture is dehydrated again and sieved to a particle size under 50 μ m. Finally, the mixture is preconditioned by cycling five times as described for the individual salts (25 % RH is used during hydration), ending in the dehydrated state for subsequent experiments.

In this study, we refer to the as-received $SrCl_2$ and $MgCl_2$ without any alterations made to their particle size as pristine salts. Preconditioned salts are these pristine salts that are cycled five times at the p-T conditions described. Ball-milled salts are pristine salts that are ball milled, sieved to $<50~\mu m$, and then cycled five times as described.

2.3. Scanning electron microscopy (SEM)

To provide insight into the microstructure and particle size of each salt before and after fabrication, SEM (Phenom XL G2) was performed at a 15 kV accelerating voltage and chamber pressure of 10 Pa. All images were taken at approximately $2000\times$ magnification, as this provided detailed particle size with minimal blurring. Conductive tape was used to prevent charging of the materials during imaging.

2.4. X-ray diffraction (XRD)

To confirm the formation of the salt mixture, powder X-ray diffraction (XRD) analysis (Rigaku Smartlab XE) was performed on the individual ball-milled salts and their binary mixture. All samples were in their dehydrated state at 105 $^{\circ}\text{C}$ (SrCl₂ and MgCl₂·H₂O). The samples were characterized at 20 angles from 10° to 60° for 30 min at 25 $^{\circ}\text{C}$ under vacuum to prevent exposure to moisture during the XRD measurement. Phase identification was performed using HighScore Plus with the PDF 4+ Database from the International Centre for Diffraction Data (ICDD).

2.5. Simultaneous thermal analysis (STA)

To quantify the energy storage density (ESD) and power density (PD) associated with the thermochemical reaction for each salt, simultaneous

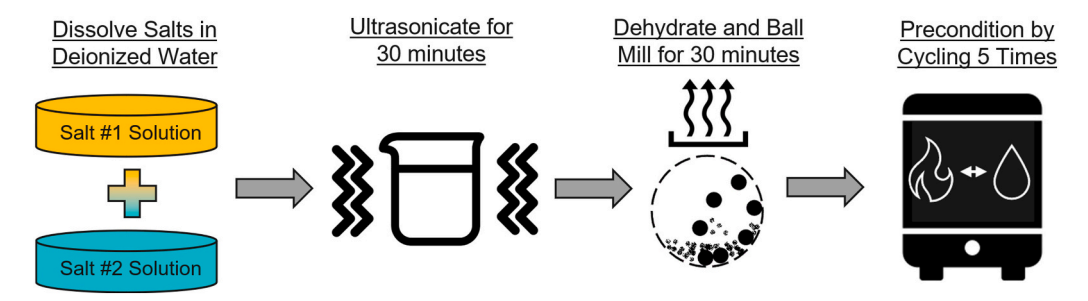


Fig. 2. Fabrication of binary salt mixtures with uniform particle size *via* ball milling and sieving to <50 μm. One cycle of preconditioning comprises dehydration at 105 °C and 0 % *RH*, followed by hydration at 25 °C and 25 % *RH*.

thermal analysis (Mettler Toledo TGA/DSC 3+) was performed and analyzed using the STARe software [47]. This STA system comprises a thermogravimetric analyzer (TGA) equipped with a humidity generator (ProUmid) that enables precise RH control in a 40 μ L open-pan aluminum crucible for mass change measurements during hydration/dehydration. Simultaneously, specific energy density (J g⁻¹) is measured using differential scanning calorimetry (DSC), with the thermal power density (W kg⁻¹) being extracted as the peak of this curve. STA characterization thus enables both hydration and dehydration measurements (cycling) to be performed at different p/RH and T without moving the sample out of the chamber.

A sample mass of 3–5 mg was used to minimize vapor diffusion resistance through the salt layer, and a flow rate of 100 mL min⁻¹ (dry nitrogen for dehydration and moist nitrogen at a specified *RH* for hydration) was used that minimizes noise in the STA signal while providing sufficient gas flow for the chemical reactions to occur – we note that these STA input parameters are based on optimal values established in our previous study that yield energy densities close to theoretical (equilibrium) predictions [20].

In the STA, all samples were initially maintained at 80 °C and 0 % RH to ensure they were in their dehydrated state after the fabrication process. We note that MgCl2 is in its dihydrate state and SrCl2 is in its anhydrous state at 80 °C; this dehydration temperature is close to the upper limit of the STA with a humidity generator attached for continuous cycling, while still being relevant for building applications [48]. The temperature was then lowered to 25 °C before increasing RH to initiate the hydration reaction (discharging step) to the hexahydrate state (MgCl₂ hydrates at 25 % RH, while SrCl₂ hydrates at 60 % RH). After the salt reached the fully hydrated state (confirmed by calculating the moles of water uptake from TGA data), the temperature was increased to 80 °C at 10 K min⁻¹ and 0 % RH to begin the dehydration reaction (charging step). The individual salts were subjected to one full hydration-dehydration cycle in its pristine, preconditioned, and ballmilled forms to quantify the effect of particle size on vapor diffusion and reaction kinetics.

Additional experiments were performed with the ball-milled $SrCl_2$ and $MgCl_2$ samples to simulate representative operating conditions in the summer and winter using ambient air (open system). Specifically, at a fixed p (\sim 19 mbar for $SrCl_2$ and 8 mbar for $MgCl_2$) the T is altered (purple diamond symbols in Fig. 1), and at a fixed T of 25 °C the p is varied (gold diamond symbols in Fig. 1). Each experiment was performed three times, with standard deviations reported as error bars to demonstrate repeatability.

The binary mixture (ball-milled form) of $SrCl_2$ and $MgCl_2$ was also characterized under the same STA dehydration and hydration conditions as the individual salts for direct comparison. In all cases, the TGA mass % data is reported as the hydration extent, α shown in Eq. (3):

$$\alpha(t) = \frac{m(t) - m_i}{m_f - m_i} \tag{3}$$

where m(t) is the mass of the sample at time t, m_i is the initial

(dehydrated) mass, and m_f is the final (hydrated) mass. For SrCl₂, α ranging from 0 to 100 % represents the transition from the anhydrous to hexahydrate state, whereas for MgCl₂ it is the transition from the dihydrate (lowest hydrate at 80 °C) to hexahydrate state.

2.6. Hygrothermal cycling

To characterize changes in material stability and reaction kinetics with smaller particle sizes and a binary mixture of the two salts, ball-milled $SrCl_2 \cdot 6H_2O$, $MgCl_2 \cdot 6H_2O$, and their binary mixture (equal mass of both salts) were subjected to a hydration-dehydration cycling study. The sample preparation and experimental conditions are the same as those mentioned in the STA section, with 20 cycles performed to enable a comparison with other reports in the literature [18,41,49]. In all cases, ESD for both hydration and dehydration, as well as PD during hydration are extracted from DSC data – these values represent the peak thermal storage density (energy and power) at the material level when minimal heat and mass transport limitations are present [41].

3. Results and discussion

We first present results for $MgCl_2$ and $SrCl_2$ as individual salts. Although these salts have been characterized in the literature, the particle size and STA characterization parameters vary widely. This necessitates establishing a baseline for the storage performance of the two salts and a comparison with their binary mixture.

3.1. Effect of particle size – structural stability

Pristine MgCl₂ and SrCl₂ vary in size and microstructure (Fig. S1), with the latter being larger and more porous. Furthermore, the salt structure evolves during cycling as shown in Fig. 3a due to volumetric expansion and contraction (crystal volume change of 45 % for MgCl₂ and 65 % for SrCl₂) that causes mechanical stresses and crack formation. In other words, hygrothermal cycling induces self-pulverization of the salts into smaller particles with increased surface area. This in turn improves the hydration rate of SrCl₂ (Fig. S2a) and MgCl₂ (Fig. S2b) over the initial 5 cycles (preconditioning). However, 5 cycles is not sufficient as self-pulverization will continue till a critical size is reached [18]. To this end, ball milling is used to consistently achieve particle sizes <50 μm. Unlike the pristine salts, cycling the ball-milled salts has no impact on the microstructure (Fig. 3a) and confirmed by the overlap in hydration rates over 5 cycles for SrCl₂ (Fig. S2c) and MgCl₂ (Fig. S2d). A larger surface area to volume ratio allows vapor to diffuse rapidly within the salt. Furthermore, the increased surface area provides more nucleation sites, thus reducing the metastable zone (i.e., energetic barrier for hydration) and facilitating the reaction.

This improvement in the rate (represented by α) with preconditioning and ball milling compared to the pristine material, is shown in Fig. 3b for SrCl₂ and 3c for MgCl₂. Specifically, ball-milled SrCl₂ reaches its hexahydrate state in 50 min while the pristine and preconditioned samples need 15 min longer owing to the larger particle

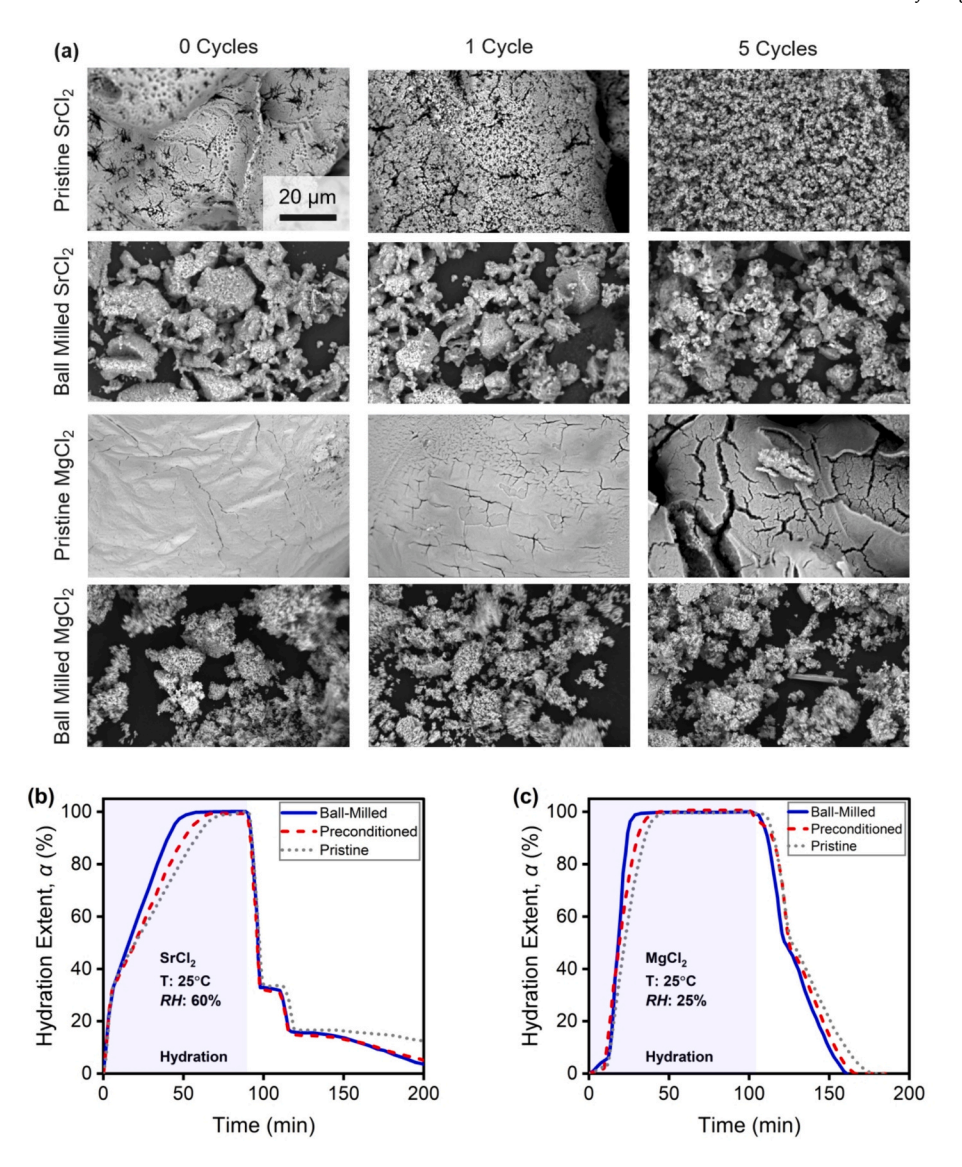


Fig. 3. (a) SEM images of as-received $SrCl_2 \cdot 6H_2O$ (500–1000 μm , Fig. S1) and $MgCl_2 \cdot 6H_2O$ (200–600 μm , Fig. S1), and after ball milling (<50 μm). Preconditioning by cycling the salts five times results in evolution of the microstructure with each hydration-dehydration cycle. All SEM images have a scale bar of 20 μm . (b) Extent of hydration (extracted from TGA data) for $SrCl_2$ and (c) $MgCl_2$ comparing the kinetics of pristine, preconditioned, and ball-milled samples during a single hydration (blue shaded region) and dehydration (unshaded region) cycle. (For interpretation of the references to colour in this figure legend, the reader is referred to the web version of this article.)

size. This effect is less pronounced in ball-milled MgCl₂ which reaches its hexahydrate state in 30 min, while its pristine and preconditioned forms hydrate at a similar rate owing to its highly hygroscopic nature. This reveals a key difference between the two salts – the SrCl₂ reaction is strongly influenced by particle size and structural stability, while MgCl₂ is dominated by hygrothermal stability challenges as we discuss later.

The enhanced reaction rate of the ball-milled samples translates to a

higher peak power density while the energy density remains largely unchanged for both salts, as summarized in Table 1. Since the energy density for hydration is lower than dehydration (which occurs at higher temperatures) and given that the hydration reaction provides the useful output (heat discharge) from the thermochemical material, subsequent results focus on the hydration behavior of the ball-milled salts and their mixture.

Table 1
Summary of the storage performance (hydration and dehydration characterized using STA) of SrCl₂ and MgCl₂ in their pristine and ball-milled forms.

Salt (Sample state)	Dehydration energy density (J g ⁻¹)	Dehydration time (min)	Hydration energy density (J g^{-1})	Hydration time (min)	Hydration peak power density (W kg^{-1})
SrCl ₂ (Pristine)	1006 ± 13	180	864 ± 34	80	980 ± 105
SrCl ₂ (Ball-milled)	1038 ± 46	97	896 ± 62	57	1010 ± 115
MgCl ₂ (Pristine)	904 ± 25	75	748 ± 48	48	670 ± 106
MgCl ₂ (Ball-milled)	1043 ± 31	55	770 ± 66	32	1303 ± 98

3.2. Effect of temperature and vapor pressure – overcoming metastability

It is well-known that temperature and vapor pressure directly impact the reaction energy and power density. For example, Fisher et al. showed that MgCl₂ has a slower hydration rate as the temperature increases (at a fixed vapor pressure), but they did not report any energy density or cycling data [50]. Clark et al. demonstrated similar results for SrCl₂, concluding that a higher vapor pressure increases the reaction rate and thermal power at a fixed temperature [49]. However, the particle size was not taken into consideration.

With our standardized fabrication process (ball-milled samples), we can quantify the effect of p and T. As expected, for $SrCl_2$ at $25\,^{\circ}C$ a higher p (\sim 12–19 mbar) is correlated with faster hydration as shown in Fig. 4a. What is interesting is that this rate more than doubles when RH increases from 50 % to 60 %, while at an RH of 40 % the reaction is incomplete (α < 100 % within the 2-hour timeframe). This is attributed to the metastable region around the phase boundary where nucleation of the hexahydrate is kinetically hindered even though it is thermodynamically favorable [16]. For MgCl₂, a higher p (\sim 5–8 mbar) is also correlated with a faster hydration rate as Fig. 4b shows, with the reaction being 95 % complete at the lower RH due to the chosen conditions being outside its metastable zone (Fig. 1). At 40 % RH however, the hydration extent increases sharply due to deliquescence of MgCl₂ (α > 100 %).

To quantify the combined effect of p and T, we introduce β as the ratio of the difference between the applied and equilibrium vapor pressures for hydration to the difference between the deliquescence and equilibrium vapor pressures at a given T, as shown in Eq. (4):

$$\beta(T) = \frac{p_{app} - p(T)_{hyd}}{p(T)_{del} - p(T)_{hyd}} \tag{4}$$

where p_{app} is the applied vapor pressure, $p(T)_{hyd}$ is the equilibrium vapor pressure at which the salt hydrates at a given T based on the phase diagram, and $p(T)_{del}$ is the vapor pressure at which the salt deliquesces for a given T based on Fig. 1. In other words, $\beta \sim 1$ represents conditions close to deliquescence (where dissolution enthalpy and ionic mobility of the wetting layer can contribute to enhanced reaction rates), whereas $\beta \sim 0$ represents conditions close to the equilibrium hydration line (where the metastable zone exists that slows down the reaction). The β value for SrCl₂ hydrating at 40 % RH is 0.28, confirming that the reaction is ratelimited at this low value. At 60 % RH however, β increases to 0.8 where the reaction proceeds to completion at a more rapid rate. For MgCl₂, as RH increases from 15 to 25 % RH, the corresponding β increases from 0.47 to 0.87 and reaction completion is more rapidly achieved.

Now, maintaining a fixed p for each salt (19 mbar for SrCl $_2$ and 8 mbar for MgCl $_2$) the effect of temperatures ranging from 20 to 40 °C is characterized. The corresponding β values are also calculated, with a higher value correlating to faster kinetics – this is evident in Fig. 4c, where SrCl $_2$ at a fixed vapor pressure of 19 mbar hydrates faster at lower temperatures, while at 40 °C it does not fully hydrate (β is negative in this case, indicating that hydration cannot occur based on the phase diagram). In contrast, MgCl $_2$ is less impacted by different temperatures as shown in Fig. 4d as all samples hydrate at similar rates owing to the conditions being outside its metastable region.

These reaction conditions and their impact on storage performance is

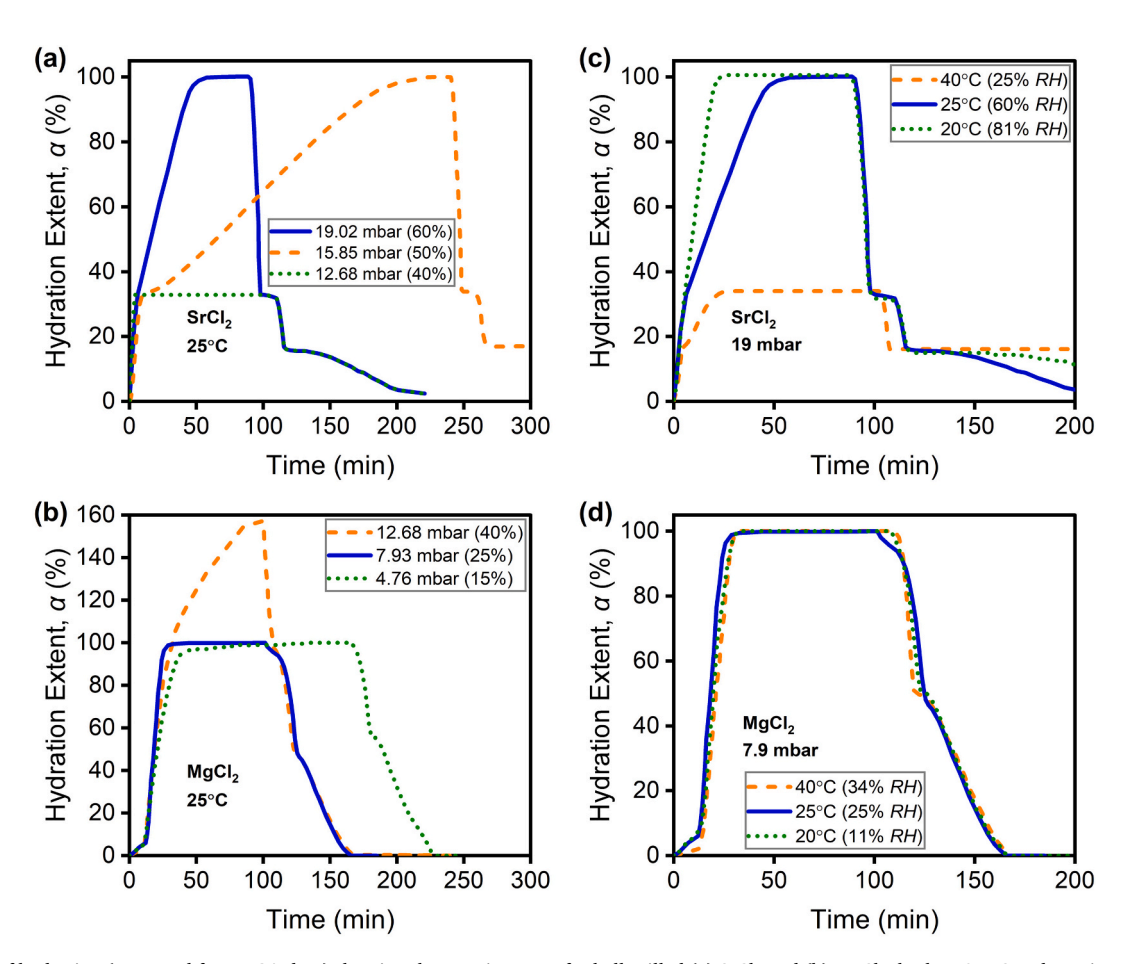


Fig. 4. Extent of hydration (extracted from TGA data) showing the reaction rates for ball-milled (a) $SrCl_2$ and (b) $MgCl_2$, both at 25 °C and varying vapor pressures, (c) $SrCl_2$ at 19 mbar and varying temperatures, and (d) $MgCl_2$ at 8 mbar and varying temperatures. These p-T values are selected based on the phase diagram (Fig. 1) of each salt. The extent of hydration, α represents one charge-discharge cycle (hydration from $SrCl_2 - SrCl_2 \cdot 6H_2O$ and $MgCl_2 \cdot 2H_2O - MgCl_2 \cdot 6H_2O$, followed by dehydration to the initial state).

summarized in Table 2 – a higher driving force $\beta \sim 0.8$ translates to higher power densities, while its impact on energy density is minimal as long as the salt can hydrate completely (while minimizing deliquescence). As such, this dimensionless metric β can be used to select the optimal conditions that maximize both energy and power density of different salts while avoiding hygrothermal instabilities (metastability and deliquescence) that occur at very low or high values of β .

3.3. Binary salt mixtures

The previous sections established that the thermochemical storage performance of $SrCl_2$ and $MgCl_2$ as individual salts can be improved through ball milling (structural stability) and hydrating at optimal conditions ($\beta \sim 0.8$). However, these salts can only be used within a narrow range of conditions (high RH for $SrCl_2$ and low RH for $MgCl_2$). This motivates the investigation of a binary salt mixture of these salts that leverages their distinct phase behaviors. We hypothesize that a mixture of these two salts can operate over a wider RH range with faster kinetics by balancing the deliquescent nature of $MgCl_2$ with the slow hydration (metastability) of $SrCl_2$. There is precedent for this approach, with Mazur et al. recently showing that the reaction hysteresis (i.e., metastable zone) and kinetics of K_2CO_3 improved with the addition of a hygroscopic salt (KF, Cs_2CO_3). However, the resulting energy density was not reported and the salts were hydrated at 40 °C which is not suitable from an application standpoint [40].

To test our hypothesis, three salt mixtures of $SrCl_2/MgCl_2$ were fabricated with mass ratios of 70/30, 50/50, and 30/70 respectively to compare samples that have a majority of one salt and an equal amount of both. Higher masses (>70 %) of $MgCl_2$ and $SrCl_2$ in the mixture resulted in deliquescence and slow (incomplete) reactions, respectively, and

Table 2 Hydration energy density and peak power density (from DSC data) for ball-milled $SrCl_2$ and $MgCl_2$ samples under different p-T conditions that impact the reaction driving force, β .

Salt (moles of H ₂ O)	Temperature (°C)	Vapor pressure (mbar), (RH)	Reaction driving force, β	Energy density (J g ⁻¹)	Peak power density (W kg ⁻¹)
Constant te	emperature, varyin	g vapor pressure	9		
$SrCl_2$	25	19.02 (60	0.80	896 \pm	1010 \pm
(0-6)		%)		62	115
		15.85 (50	0.54	955 \pm	775 \pm
		%)		50	50
		12.68 (40	0.28	238 \pm	433 \pm
		%)		44 ^a	118 ^a
$MgCl_2$	25	12.68 (40	1.28	$1209 \pm$	$1440 \; \pm$
(2-6)		%)		22^{b}	29 ^b
		7.93 (25 %)	0.87	770 \pm	$1303~\pm$
				66	98
		4.75 (15 %)	0.47	744 \pm	$668 \pm$
				12	11
Constant v	apor pressure, vary	ving temperature	3		
SrCl ₂	20	(81 %)	1.27	871 \pm	$1220~\pm$
(0-6)	20	(01 /0)	1.2,	22	41
(0 0)	25	19.02 (60	0.80	896 ±	1010 ±
	20	%)	0.00	62	115
	40	(26 %)	-0.34	283 ±	505 ±
		(20 70)	0.0 1	22ª	91ª
$MgCl_2$	20	(34 %)	1.18	793 ±	1120 ±
(2–6)	20	(0 1 70)	1.10	21	8
(= 0)	25	7.93 (25 %)	0.87	770 ±	1303 ±
		(20 70)		66	98
	40	(11 %)	0.29	902 ±	$1123 \pm$
		,		25	74

^a Represents incomplete hydration with a corresponding low energy and power density.

were not considered for further analysis. Each mixture was hydrated at 25 °C and 40 % RH (note that at these conditions, MgCl₂ by itself deliquesces as shown in Fig. 4b and SrCl₂ by itself does not fully hydrate as shown in Fig. 4a within the 1.5-hour timeframe). This was followed by dehydration at 80 °C and 0 % RH of all three mixtures. One such hydration-dehydration cycle is shown in Fig. 5, with the 30/70 mixture of SrCl₂/MgCl₂ experiencing deliquescence and forming a salt solution ($\alpha > 100$ %) owing to the large amount of MgCl₂ present. On the other hand, the 70/30 mixture only achieves a hydration extent of 67 %, and a correspondingly low energy density of 450 J g $^{-1}$. This can be attributed to the incomplete hydration of SrCl₂ (to its dihydrate state) as the reaction conditions are within the metastable region. The 50/50 mixture of SrCl₂/MgCl₂ hydrates fully ($\alpha = 100$ %), achieving a storage density of 790 J g $^{-1}$.

To provide insight into the behavior of the 50/50 mixture compared to its constituent salts, the ball-milled salts and their 50/50 mixture were subjected to varying *RH* at 25 °C in an environmental chamber for 24 h. Fig. 6 shows images of the resulting three samples, with MgCl₂ forming a solution above 30 % *RH* that after dehydration forms an agglomerated block (see inset image). The 50/50 mixture is still in powder form at these conditions, with some wetting visible at 60 % *RH* due to the deliquescence of MgCl₂. However, a heterogenous mixture (*i.e.*, a slurry) is formed instead of a liquid solution owing to the presence of SrCl₂, which once dehydrated is in powder form with less agglomeration compared to MgCl₂ by itself (see inset image). The 50/50 mixture thus shows promise as a new thermochemical storage material compared to its constituent salts.

To verify that mixing of two salts is purely a physical process without new compounds being formed, XRD measurements were performed on the dehydrated salts (SrCl₂·H₂O, MgCl₂·2H₂O, and 50/50 mixture) – as shown in Fig. 7a, strong diffraction peaks of SrCl2·H2O are mainly located at $\sim \! 16^\circ, \, 20^\circ, \, 26^\circ, \, 31^\circ, \, 33^\circ, \, 38^\circ$ and $44^\circ, \,$ which is in agreement with literature [41]. As for MgCl₂·2H₂O, the characteristic peaks are at $\sim 16^{\circ}, 20^{\circ}, 22^{\circ}, 26^{\circ}, 29^{\circ}, 32^{\circ}, 41^{\circ}$ and 43° . In the 50/50 mixture, most of the peaks correspond to the crystalline structure of either SrCl₂·H₂O or MgCl₂·2H₂O, which confirms the presence of the individual salts with no byproducts formed (i.e., due to ion exchange or chemical reactions between the two salts). Additional peaks in the mixture may be attributed to multiple hydrates of the individual salts [20]. Mixing being a physical process is also confirmed from one hydration-dehydration cycle of the 50/50 sample – as shown in Fig. 7b, both the hydration and dehydration slope changes can be matched with that of the individual salts (see inset plots of SrCl2 and MgCl2).

Since the individual salts and their mixture have similar particle sizes

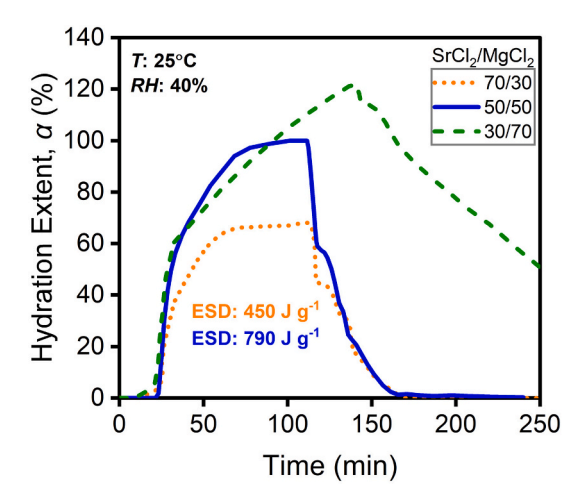


Fig. 5. Hydration extent and energy density values of three $SrCl_2/MgCl_2$ mixtures with varying amounts of each salt. Hydration is performed at 25 °C and 40 % RH, followed by dehydration at 80 °C and 0 % RH.

^b Represents deliquescence during hydration that contributes dissolution enthalpy in addition to solid-gas reaction enthalpy.

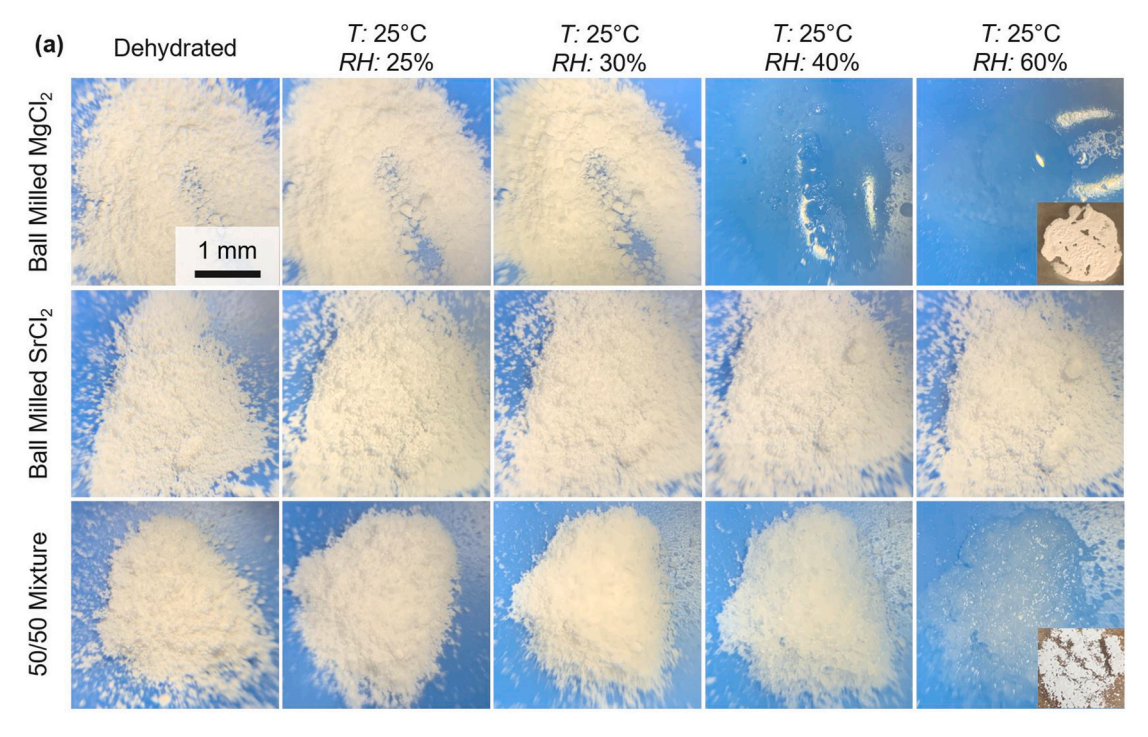


Fig. 6. Images of ball-milled powders of MgCl₂, SrCl₂ and their 50/50 mixture at different *RH* values from 25 to 60 % at a fixed temperature of 25 °C. All images have a scale bar of 1 mm and were captured after hydrating at the specified *RH* for 24 h. Insets represent the salts after dehydration at 105 °C overnight.

and preconditioning steps in this study, a direct comparison of their storage performance can now be made for one hydration-dehydration cycle at 25 °C and varying RH values. This is summarized in Table 3, which shows that the 50/50 mixture of $SrCl_2/MgCl_2$ hydrates across the 25–60 % RH range unlike its constituent salts – this covers typical outdoor conditions, making the mixture promising for thermochemical heat discharge during both summer and winter months [51]. Importantly, the $SrCl_2/MgCl_2$ binary mixture achieves a specific storage density above 1100 J g $^{-1}$ (~300 Wh kg $^{-1}$) and peak thermal power output over ~1.4 kW kg $^{-1}$, which is suitable to offset thermal loads in a building. We note that these numbers are at the material level and will change depending on the salt bed porosity and permeability in a reactor or storage system.

3.4. Mechanisms and design rules for salt mixtures

Having established that mixing is a physical process and that the 50/ 50 mixture of SrCl₂/MgCl₂ maintains the inherent phase behavior of its constituent salts, we turn to understand the different contributions to its energy density at different RH values. The water vapor uptake (extracted from TGA data and defined as the mass of water sorbed per gram of dehydrated salt) is shown in Fig. 8a. At 25 % RH, MgCl₂ in the mixture hydrates to its hexahydrate state while SrCl₂ only reaches its dihydrate state. The corresponding ESD is 626 J g^{-1} , which is lower than that of MgCl₂ alone at the same conditions (770 J g⁻¹) owing to the presence of SrCl₂. At 40 % RH, MgCl₂ in the mixture fully hydrates and deliquesces (as shown in Fig. 6), with this wetting layer leading to dissolution that increases ESD of the mixture to 790 J g⁻¹. At these conditions, the water uptake of the mixture (\sim 0.55 g_{water}/g_{salt}) shown in Fig. 8a almost exactly matches the average of the water uptakes of the deliquesced $MgCl_2$ (0.61 g_{water}/g_{salt}) and $SrCl_2 \cdot 6H_2O$ (0.51 g_{water}/g_{salt}) at the same conditions (Supplementary Note 1, Fig. S6a). This suggests that both salts within the mixture have reached their fully hydrated state – this is surprising as we do not expect SrCl2 by itself to reach its hexahydrate at 25 $^{\circ}\text{C}$ and 40 % RH owing to this being in the metastable zone where the solid-gas hydration reaction is rate limited (supported by the slow mass gain of SrCl₂ in Figs. 4a and S6a). We hypothesize that this is because the deliquescence of MgCl₂ creates a wetting layer that helps overcome the energetic barrier for hydration of SrCl2 in its vicinity within the 1.5 h of this measurement. When the vapor pressure is increased to 60 % RH, energy density increases significantly to 1120 J g⁻¹, with more wetting being observed (a heterogenous mixture or slurry as shown in Fig. 6). This is attributed both to SrCl₂ within the mixture being able to fully reach its hexahydrate state without any kinetic hinderance, and the dissolution enthalpy of MgCl₂ sharply increasing the water uptake shown in Fig. 8a. Thus, the performance of the binary mixture can be explained by accounting for the complete hydration of MgCl₂ and some hydration of SrCl₂ depending on the vapor pressure (both of which contribute solid-gas reaction enthalpy), as well as some dissolution due to the deliquescent nature of MgCl2 (which contributes solution enthalpy). The mechanism is illustrated in Fig. 8b revealing the benefit of combining two salts with distinct phase behavior by achieving complete hydration while preventing full deliquescence, and this is consistent with literature reports on other salts [16,40]. Direct observation of the formation of the wetting layer in different regions of the mixture can be obtained from in situ SEM and XRD studies to validate the hypothesized mechanism - this is the focus of ongoing work and will be reported in a subsequent manuscript.

3.5. Cycling performance – hygrothermal stability

Finally, we report the performance of the two salts and their binary mixture when subjected to 20 hydration-dehydration cycles as is typically done in literature [18,41,49]. For each cycle, sufficient time (1.5–3 h) was provided to ensure that hydration (at 25 °C and different RH values depending on the sample) and dehydration (80 °C and 0 % RH for all samples) reactions approach completion (Fig. S3 – mass % plateaus over time). The corresponding energy and power density values for each cycle are obtained from the DSC, with the dehydration energy density being higher as it occurs at a higher temperature than hydration (Figs. S4 and S5).

For the ball-milled SrCl₂, Fig. 9a shows that cycling has a negligible impact as the water vapor uptake (at 60 % RH) is relatively unchanged around $0.6 \text{ g}_{\text{water}}/\text{g}_{\text{salt}}$ (dehydrated) and the energy density is within 95 % of its initial value (ESD of each cycle is normalized to the first cycle

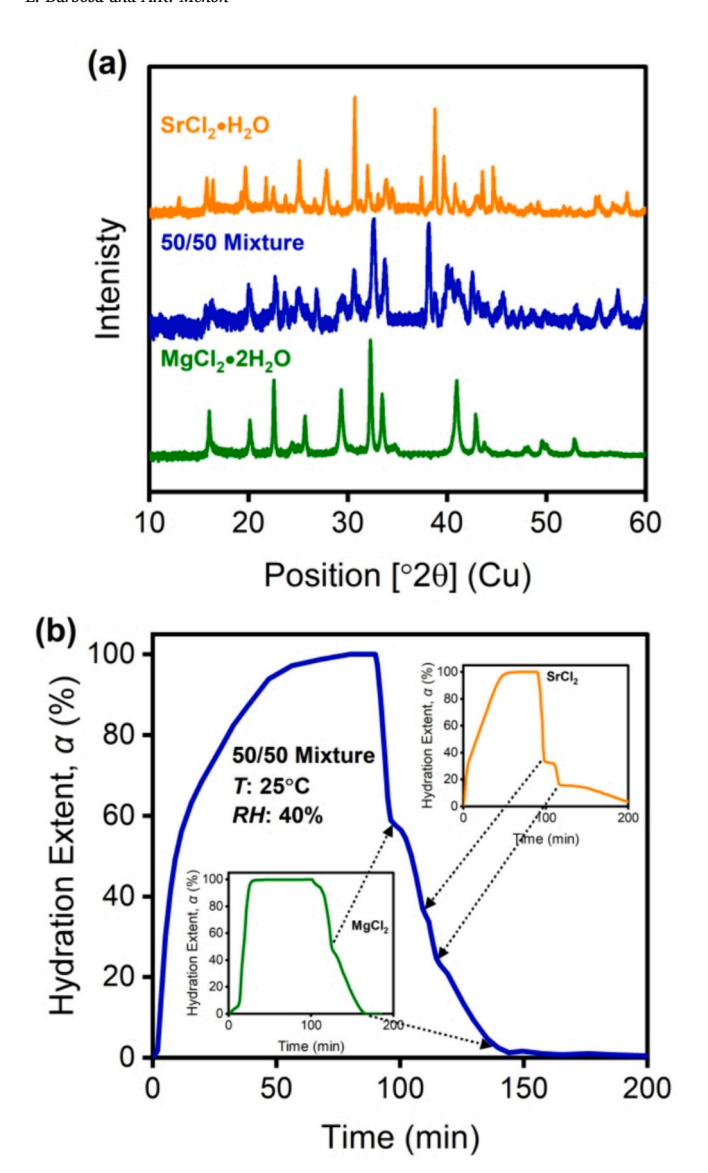


Fig. 7. (a) Powder XRD patterns of $SrCl_2 \cdot H_2O$, $MgCl_2 \cdot 2H_2O$, and their 50/50 mixture. Each sample was dehydrated at 105 °C before measurements were performed under vacuum. (b) Hydration extent (extracted from TGA data) of the 50/50 mixture at 40 % *RH* and 25 °C, with arrows showing combined features from the individual salts of $SrCl_2$ and $MgCl_2$.

Table 3 Hydration energy density and peak power density of ball-milled SrCl₂, MgCl₂, and their 50/50 mixture by weight.

Salt	Hydration conditions (<i>T</i> ; <i>RH</i>)	Hydration energy density (J g ⁻¹)	Hydration peak power density (W kg^{-1})	
SrCl ₂ 25 °C; 25 % (Incomplete		(Incomplete hydration	hydration)	
	25 °C; 40 %	238 ± 44	433 ± 118	
	25 °C; 60 %	896 ± 62	1010 ± 115	
$MgCl_2$	25 °C; 25 %	770 ± 66	1303 ± 98	
	25 °C; 40 %	1209 ± 22	1440 ± 29	
	25 °C; 60 %	(Deliquesces)		
50/50	25 °C; 25 %	626 ± 54	1000 ± 110	
mixture	25 °C; 40 %	790 ± 37	1230 ± 94	
	25 °C; 60 %	1120 ± 115	1360 ± 120	

value of 890 J g^{-1}). This is attributed to the fact that ball milling results in a structurally stable salt as previously discussed. Furthermore, the high *DRH* of this salt ensures that it is hygrothermally stable during continuous hydration-dehydration (confirmed by the overlap in the TGA

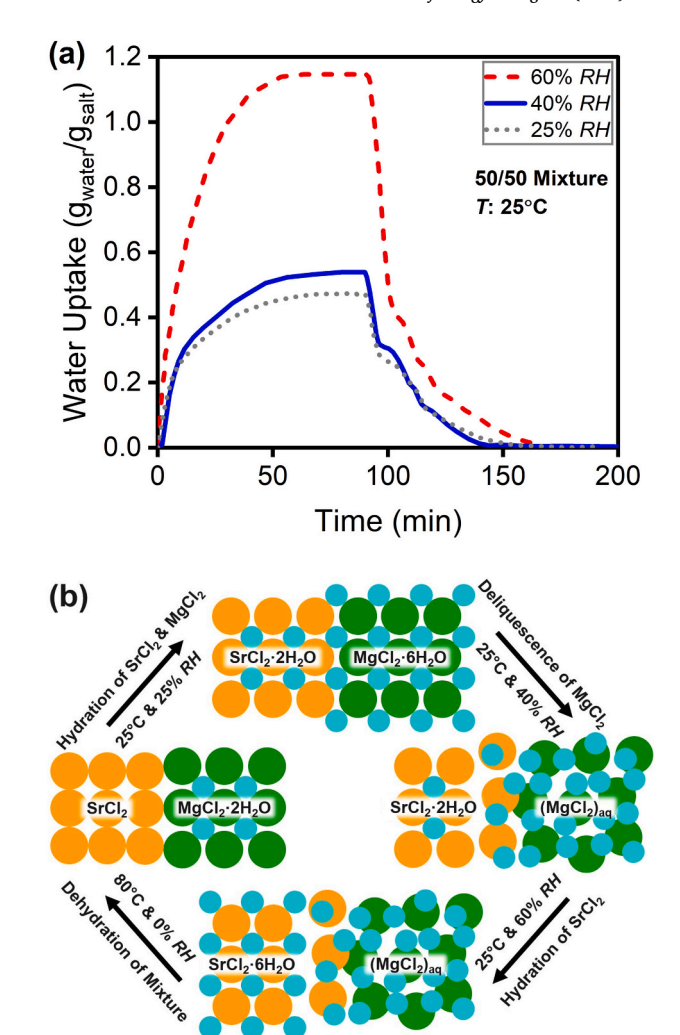


Fig. 8. (a) Water uptake of the 50/50 mixture of $SrCl_2/MgCl_2$ hydrating at 25 °C and different *RH* values. (b) Illustration of the mechanism in a binary salt mixture, where there is a combined solid-gas reaction enthalpy and dissolution enthalpy associated with the hygroscopic nature of $MgCl_2$ that promotes $SrCl_2$ hydration.

curves for each cycle in Fig. S3a). For MgCl₂ however, cycling results in a significant reduction in the mass uptake (at 25 % RH) and energy density as shown in Fig. 9b, only retaining about 60 % of its initial energy density of 770 J g⁻¹ after 20 cycles. This is because the highly hygroscopic nature of MgCl2 causes deliquescence during hydration, and dehydrating it yields an agglomerated salt. As a result, the porosity and surface area are reduced which is essential for vapor to diffuse and react with the salt (confirmed by the large variation in the TGA curves for each cycle in Fig. S3b). This is one of the key reasons that MgCl₂ by itself cannot be used as a practical TCM despite its low cost and high ESD. In comparison, the 50/50 mixture under these same cycling conditions (25 % RH) retains \sim 80 % of its initial energy density of 626 J g⁻¹ after 20 cycles as shown in Fig. 9c. Even at a higher RH of 40 %, the mixture retains \sim 77 % of its initial energy density of 790 J g⁻¹ after 20 cycles as shown in Fig. 9d, as long as sufficient time is provided for the mixture to dehydrate (1.5 h to de/hydrate at 25 % RH, and 3 h at 40 % RH (Supplementary Note 2, Fig. S7a). The decrease in energy density with cycling is directly related to the decrease in water uptake, as MgCl2 within the mixture agglomerates to some extent but it is mediated by the presence of SrCl2 as discussed previously.

Overall, the 50/50 mixture demonstrates improved cycling stability compared to $MgCl_2$ alone while hydrating over a larger RH range compared to $SrCl_2$ alone. These results present an improvement

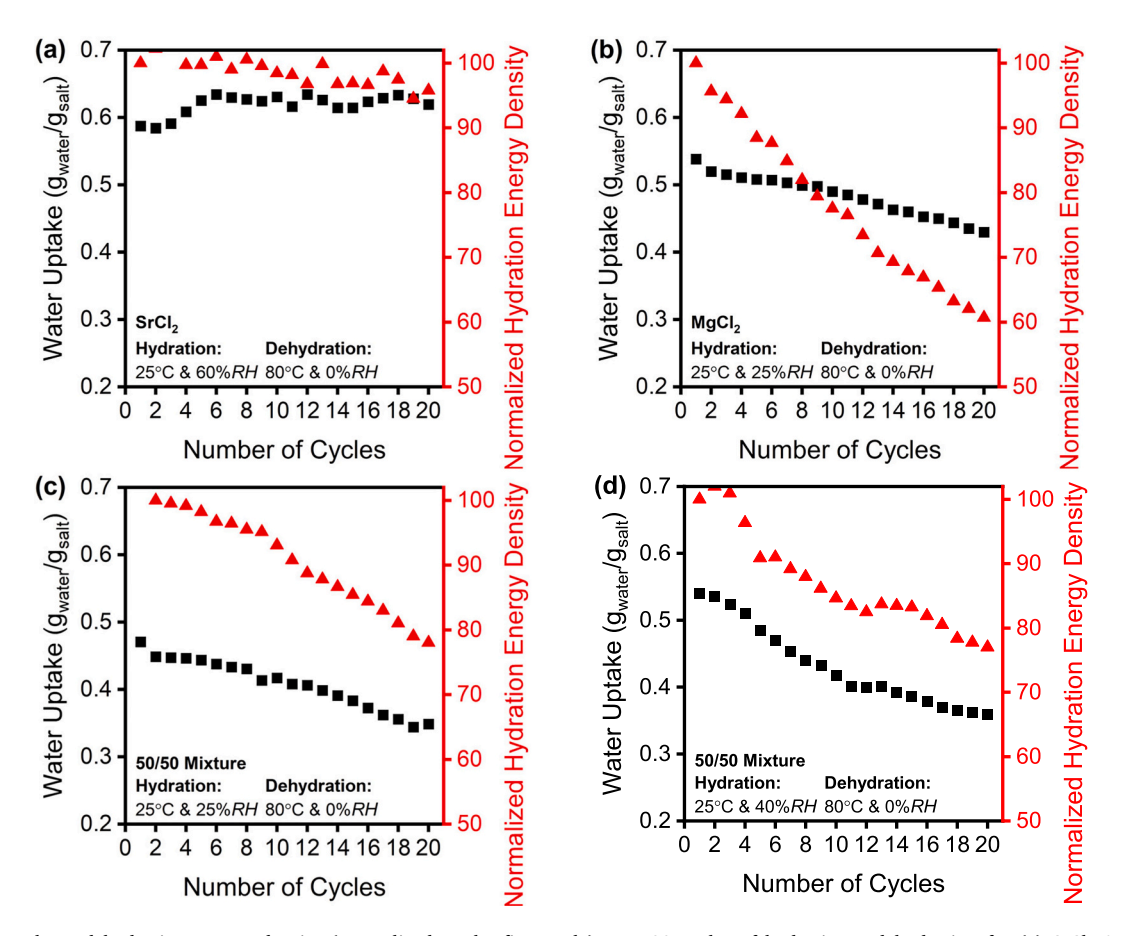


Fig. 9. Water uptake and hydration energy density (normalized to the first cycle) over 20 cycles of hydration – dehydration for (a) $SrCl_2 \cdot 6H_2O - SrCl_2$, (b) $MgCl_2 \cdot 6H_2O - MgCl_2 \cdot 2H_2O$, (c) 50/50 mixture hydrating at 25 °C and 25 % *RH* and (d) 50/50 mixture hydrating at 25 °C and 40 % *RH*. Note that the reaction time was maintained at 1.5 h in (a) – (c) and increased to 3 h in (d).

compared to two literature studies on binary salt mixtures that report cycling data (Fig. S7b). Specifically, a 50/50 mixture of MgSO₄/ZnSO₄ shows a significant drop in hydration energy density to 60% of the initial value [37], while an 80/20 mixture of SrCl₂/MgSO₄ drops to 75% of its initial energy density after 20 cycles [41]."

4. Conclusions

The material-level performance of two thermochemical salts with distinct phase behavior and hygrothermal stability, $SrCl_2$ and $MgCl_2$, were characterized. The focus was on their hydration behavior due to its complexity as well as importance for extracting heat from the storage material. Experiments on the individual salts revealed that they can only hydrate in a narrow RH range, and this motivated the development of their binary salt mixture. The main conclusions of this work are as follows:

- Ball milling salts to micron-sized particles ($<50~\mu m$) and preconditioning by cycling five times (dehydration-hydration) minimizes vapor transport resistance and improves reaction kinetics. This yields a structurally stable salt with enhanced reaction rates reported as the hydration extent, α .
- The optimal p T conditions for the reaction can be characterized in terms of a hydration driving force β , with a value \sim 0.8 resulting in higher power densities with minimal impact on energy density as long as the salt hydrates completely at those conditions.
- The addition of a highly hygroscopic and deliquescent salt (MgCl₂) to the mixture improves reaction kinetics by overcoming the

- metastability of the other salt (SrCl₂). This is hypothesized to be due to the formation of a wetting layer and dissolution enthalpy.
- Mixtures comprising a common ion (chloride in this case) interact only physically, minimizing the likelihood of side reactions and formation of new compounds.
- The binary SrCl₂/MgCl₂ mixture operates over a wider range of *RH* (25–60 % at 25 °C) compared to its constituent salts (<30 % for MgCl₂ and >60 % for SrCl₂). A 50/50 (by mass) mixture of this salt exhibits an energy storage capacity of >1100 J g⁻¹ that is maintained within 80 % over 20 cycles. This represents an improvement over other binary mixtures reported in the literature, but further improvements in cycling stability are needed for building applications.

CRediT authorship contribution statement

Erik Barbosa: Writing – review & editing, Writing – original draft, Visualization, Validation, Software, Methodology, Investigation, Formal analysis, Data curation. **Akanksha K. Menon:** Writing – review & editing, Writing – original draft, Supervision, Resources, Project administration, Funding acquisition, Conceptualization.

Declaration of competing interest

The authors declare that they have no known financial interests/ personal relationships which may be considered as potential competing interests.

Data availability

Supporting data is available in the Supplementary Information, and additional data will be made available upon request by contacting the corresponding author.

Acknowledgements

This material is based upon work supported by the National Science Foundation under Grant No. CBET-2238705. This work was performed in part at the Georgia Tech Institute for Electronics and Nanotechnology, a member of the National Nanotechnology Coordinated Infrastructure (NNCI), which is supported by the National Science Foundation under Grant No. ECCS-2025462. EB acknowledges financial support from the National Science Foundation Graduate Research Fellowship and the President's Fellowship at Georgia Tech. The authors thank Kelsey Cavallaro for XRD measurements, Lucas Nicewander and Ian Kwuan for sample preparation, and Jordan Kocher for discussions related to the salt mixtures.

Appendix A. Supplementary data

Supplementary data to this article can be found online at https://doi.org/10.1016/j.est.2024.111916.

References

- M.M. Rana, et al., Applications of energy storage systems in power grids with and without renewable energy integration — a comprehensive review, Journal of Energy Storage (2023) 68.
- [2] J.A. Dowling, et al., Role of long-duration energy storage in variable renewable electricity systems, Joule 4 (9) (2020) 1907–1928.
- [3] A. Henry, R. Prasher, A. Majumdar, Five thermal energy grand challenges for decarbonization, Nat. Energy 5 (9) (2020) 635–637.
- [4] T. Gilbert, et al., Heat source and application-dependent levelized cost of decarbonized heat, Joule 7 (1) (2023) 128–149.
- [5] Residential Energy Consumption Survey, Available from: https://www.eia.gov/consumption/residential/index.php.
- [6] J. Lizana, et al., Advances in thermal energy storage materials and their applications towards zero energy buildings: a critical review, Appl. Energy 203 (2017) 219–239.
- [7] P. Tatsidjodoung, N. Le Pierrès, L. Luo, A review of potential materials for thermal energy storage in building applications, Renew. Sust. Energ. Rev. 18 (2013) 327–349
- [8] G. Sadeghi, Energy storage on demand: thermal energy storage development, materials, design, and integration challenges, Energy Storage Materials 46 (2022) 192–222.
- [9] J. Romaní, et al., Evaluation of energy density as performance indicator for thermal energy storage at material and system levels, Appl. Energy 235 (2019) 954–962.
- [10] W. Li, et al., Salt hydrate-based gas-solid thermochemical energy storage: current progress, challenges, and perspectives, Renew. Sust. Energ. Rev. 154 (2022).
- [11] X. Chen, et al., State of the art on the high-temperature thermochemical energy storage systems, Energy Convers. Manag. 177 (2018) 792–815.
- [12] J. Lin, et al., Applications of low-temperature thermochemical energy storage systems for salt hydrates based on material classification: a review, Sol. Energy 214 (2021) 149–178.
- [13] R.-J. Clark, A. Mehrabadi, M. Farid, State of the art on salt hydrate thermochemical energy storage systems for use in building applications, Journal of Energy Storage (2020) 27.
- [14] Y. Zhang, R. Wang, Sorption thermal energy storage: concept, process, applications and perspectives, Energy Storage Materials 27 (2020) 352–369.
- [15] P.A.J. Donkers, et al., A review of salt hydrates for seasonal heat storage in domestic applications, Appl. Energy 199 (2017) 45–68.
 [16] L.-C. Sögütoglu, et al., Understanding the hydration process of salts: the impact of a
- [16] L.-C. Sögütoglu, et al., Understanding the hydration process of salts: the impact of a nucleation barrier, Cryst. Growth Des. 19 (4) (2019) 2279–2288.
- [17] N. Mazur, et al., Impact of polymeric stabilisers on the reaction kinetics of SrBr2, Sol. Energy Mater. Sol. Cells 238 (2022).
- [18] A. Martin, et al., Particle size optimization of thermochemical salt hydrates for high energy density thermal storage, Energy Environ. Mater. 7 (2) (2023) 12544.
- [19] J. Aarts, et al., Diffusion limited hydration kinetics of millimeter sized salt hydrate particles for thermochemical heat storage, Journal of Energy Storage 47 (2022) 103554.
- [20] E. Barbosa, A.K. Menon, Thermodynamic and kinetic characterization of salt hydrates for thermochemical energy storage, MRS Communications 12 (5) (2022) 678–685.

- [21] R.-J. Clark, et al., Experimental screening of salt hydrates for thermochemical energy storage for building heating application, Journal of Energy Storage (2022) 51
- [22] J. Houben, et al., K2CO3 in closed heat storage systems, Renew. Energy 166 (2020)
- [23] L.C. Sögütoglu, et al., In-depth investigation of thermochemical performance in a heat battery: cyclic analysis of K2CO3, MgCl2 and Na2S, Appl. Energy 215 (2018) 159–173.
- [24] J. Xu, et al., Dehydration kinetics and thermodynamics of magnesium chloride hexahydrate for thermal energy storage, Sol. Energy Mater. Sol. Cells 219 (2021).
- [25] W. Zhao, et al., Morphology and thermal properties of calcium alginate/reduced graphene oxide composites, Polymers (Basel) 10 (9) (2018).
- [26] B. Michel, P. Neveu, N. Mazet, Comparison of closed and open thermochemical processes, for long-term thermal energy storage applications, Energy 72 (2014) 702–716.
- [27] M.H. Nguyen, et al., Thermochemical sorption heat storage: investigate the heat released from activated carbon beads used as porous host matrix for MgSO₄ salt, Journal of Energy Storage (2023) 59.
- [28] M.A.R. Blijlevens, et al., A study of the hydration and dehydration transitions of SrCl2 hydrates for use in heat storage, Sol. Energy Mater. Sol. Cells 242 (2022).
- [29] A. Shkatulov, et al., Core-shell encapsulation of salt hydrates into mesoporous silica shells for thermochemical energy storage, ACS Applied Energy Materials 3 (7) (2020) 6860–6869.
- [30] B.G.P. van Ravensteijn, et al., Encapsulation of salt hydrates by polymer coatings for low-temperature heat storage applications, ACS Applied Polymer Materials 3 (4) (2021) 1712–1726.
- [31] P.A. Kallenberger, et al., Alginate-derived salt/polymer composites for thermochemical heat storage, Advanced Sustainable Systems 2 (7) (2018).
- [32] A. Cammarata, et al., Hybrid strontium bromide-natural graphite composites for low to medium temperature thermochemical energy storage: formulation, fabrication and performance investigation, Energy Convers. Manag. 166 (2018) 233–240.
- [33] W. Li, et al., Development and characteristics analysis of salt-hydrate based composite sorbent for low-grade thermochemical energy storage, Renew. Energy 157 (2020) 920–940.
- [34] J. Cot-Gores, A. Castell, L.F. Cabeza, Thermochemical energy storage and conversion: a-state-of-the-art review of the experimental research under practical conditions, Renew. Sust. Energ. Rev. 16 (7) (2012) 5207–5224.
- [35] M. Gaeini, et al., Characterization of microencapsulated and impregnated porous host materials based on calcium chloride for thermochemical energy storage, Appl. Energy 212 (2018) 1165–1177.
- [36] Q. Miao, et al., MgSO4-expanded graphite composites for mass and heat transfer enhancement of thermochemical energy storage, Sol. Energy 220 (2021) 432–439.
- [37] A.U. Rehman, M. Khan, Z. Maosheng, Hydration behavior of MgSO4–ZnSO4 composites for long-term thermochemical heat storage application, Journal of Energy Storage (2019) 26.
- [38] H. Ait Ousaleh, et al., New hybrid graphene/inorganic salt composites for thermochemical energy storage: synthesis, cyclability investigation and heat exchanger metal corrosion protection performance, Sol. Energy Mater. Sol. Cells 215 (2020)
- [39] K. Posern, C. Kaps, Calorimetric studies of thermochemical heat storage materials based on mixtures of MgSO4 and MgCl2, Thermochim. Acta 502 (1–2) (2010) 73-76
- [40] N. Mazur, et al., A systematic deliquescent additive selection approach for enhancement of reaction kinetics of thermochemical heat storage materials, Sol. Energy Mater. Sol. Cells 263 (2023).
- [41] W. Li, M. Zeng, Q. Wang, Development and performance investigation of MgSO4/ SrCl2 composite salt hydrate for mid-low temperature thermochemical heat storage, Sol. Energy Mater. Sol. Cells 210 (2020).
- [42] H.U. Rammelberg, et al., Thermochemical heat storage materials performance of mixed salt hydrates, Sol. Energy 136 (2016) 571–589.
- [43] A. Serrano-Aroca, J.F. Ruiz-Pividal, M. Llorens-Gamez, Enhancement of water diffusion and compression performance of crosslinked alginate films with a minuscule amount of graphene oxide, Sci. Rep. 7 (1) (2017) 11684.
- [44] K.E. N'Tsoukpoe, et al., A systematic multi-step screening of numerous salt hydrates for low temperature thermochemical energy storage, Appl. Energy 124 (2014) 1–16.
- [45] L. Glasser, Thermodynamics of inorganic hydration and of humidity control, with an extensive database of salt hydrate pairs, J. Chem. Eng. Data 59 (2) (2014) 526–530
- [46] P. PatNaik, Handbook of Inorganic Chemical, 1 ed., McGraw-Hill, 2002.
- [47] N.F.A. Zainal, et al., Thermal analysis: basic concept of differential scanning calorimetry and thermogravimetry for beginners, Chemistry Teacher International 3 (2) (2021) 59–75.
- [48] M. Richter, et al., A systematic screening of salt hydrates as materials for a thermochemical heat transformer, Thermochim. Acta 659 (2018) 136–150.
- [49] R.-J. Clark, M. Farid, Hydration reaction kinetics of SrCl2 and SrCl2-cement composite material for thermochemical energy storage, Sol. Energy Mater. Sol. Cells 231 (2021).
- [50] R. Fisher, Y. Ding, A. Sciacovelli, Hydration kinetics of K2CO3, MgCl2 and vermiculite-based composites in view of low-temperature thermochemical energy storage, Journal of Energy Storage (2021) 38.
- [51] Goddard Earth Sciences Data and Information Services Center, Available from: https://disc.gsfc.nasa.gov/.